Point defects in the NiAl(100) surface

2009 J. Phys.: Condens. Matter 21 134007

(http://iopscience.iop.org/0953-8984/21/13/134007)

J. Phys.: Condens. Matter **21** (2009) 134007 (6pp) doi:10.1088/0953-8984/21/13/134007

Point defects in the NiAl(100) surface

D Lerch, K Dössel, L Hammer and S Müller

Lehrstuhl für Festkörperphysik, Universität Erlangen-Nürnberg, Staudtstrasse 7, D-91058 Erlangen, Germany

E-mail: stefan.mueller@physik.uni-erlangen.de

Received 31 October 2008, in final form 2 November 2008
Published 12 March 2009
Online at stacks.iop.org/JPhysCM/21/134007

Abstract

The stability of various point defects in NiAl(100) has been investigated by first-principles calculations. For Al-rich surfaces, Ni vacancies within the first Al layer are energetically most favourable. For Ni-rich surfaces, so-called double defects, consisting of both Ni-antisite atom in the first Al layer and a Ni vacancy within the second Ni layer, form the configuration of lowest energy, superior to singular Ni antisites. An additional and significant energy gain is found in both cases by mutual lateral interaction of the defects, when they are arranged in the diagonal direction. Respective c($\sqrt{2} \times 3\sqrt{2}$)R45° ordered configurations were found as the most stable structures. A 50:50 mixture of both defect types turns out to be even lower in energy than the ideal Al-terminated NiAl(100) surface, proving the latter to be metastable only. This is in line with the often reported inability in experiments to prepare ideal NiAl(100) surfaces.

1. Introduction

In 2002, Klaus Heinz and his group were able to explain the experimentally found unusual segregation behaviour of the B2-CoAl(100) surface by considering the key role of constitutional defects for the surface structure [1]. Small deviations from the ideal stoichiometry in an extended region below the surface or in the bulk can crucially shape surface segregation in intermetallic compounds—completely unlike the behaviour of the more often studied disordered alloys [2]. The situation becomes even more complex when different types of point defects come into play, as in the case of NiAl(100). In its ground state, this bimetallic phase forms a B2 structure, which is also referred to as a CsCl structure. Ideally, the (100) surface of a B2 structure is formed by alternating, quadratic layers of its two constituents. In the case of nickel and aluminium, this results in an interlayer distance of half the lattice constant $d_0 = \frac{a_0}{2} = 1.445$ Å. Two different surface terminations are possible for an ideal NiAl(100)-(1 × 1) surface: one where the top layer consists entirely of nickel and another where an aluminium layer terminates the surface.

At first glance, it appears that the atomic structure of this surface must be simple and well defined. Surprisingly, experimental studies lead to contradictory results. In their LEED study, Davis and Noonan [3, 4] find that the NiAl(100)-(1 × 1) surface is terminated by an aluminium layer. They also remark that diffuse intensities suggest that remnants of reconstructed domains are present. Using LEIS, Mullins and Overbury [5] claim a c($\sqrt{2} \times 3\sqrt{2}$)R45° phase where Al atoms in every third diagonal row of the first layer are substituted by Ni, as illustrated in figure 1. They also report that this surface phase can be annealed to exhibit laterally a (1 × 1) structure, however still containing $0.22 \pm 0.07\%$ of randomly distributed Ni atoms. In contrast to this, the NICISS study of Blum, Ahlberendt and Niehus [6] determines the c($\sqrt{2} \times 3\sqrt{2}$)R45° structure to be formed by an Al top layer with diagonal rows of vacancies rather than Ni atoms. This surface is reported to be formed most clearly for annealing temperatures around 800 K, whereas annealing below 500 K produces a (1 × 1) phase, terminated by an Al layer, including a large quantity of point defects. Moreover, for an annealing temperature at 1400 K, another (1 × 1) phase, which is terminated by an Ni layer, is also observed and attributed to be the result of Al sublimation.

As mentioned above, a possible explanation for the existence of these contradictory results was given in [1]. It was further speculated that this might also hold for surfaces of NiAl, where the B2 phase extends to both Ni- and Al-rich sides of the phase diagram being associated with either Ni-antisite atoms on the Al sublattice or vacancies within the Ni sublattice. Hence, depending on the exact stoichiometry of the crystal used for the investigation and the surface preparation procedure applied in this study, very different equilibrium surface compositions may result. The dependence of the surface structure of NiAl(100) on the exact near-surface composition was recently studied in detail again in the group of Klaus Heinz [7], where an Al-depleted surface generated by preferential sputtering and high temperature annealing was covered by an Al film. Subsequently, the

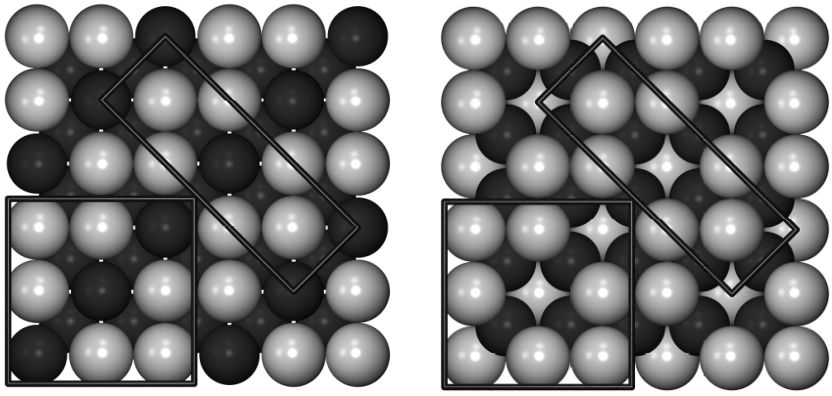

Figure 1. Illustration of the two c($\sqrt{2} \times 3\sqrt{2}$)R45° structures, which are reported in the literature: a diagonal ordering of Ni antisites [5] (left) or of Al vacancies [6] (right). Both structures can either be represented within the minimal rectangular surface unit cell or within a square (3×3) unit cell. For numerical reasons, the latter was used for the *ab initio* calculations.

near-surface composition could continuously be altered via progressive thermal annealing and reaction. In the course of this investigation indeed two c($\sqrt{2} \times 3\sqrt{2}$)R45° phases were found for both the Al-rich and Al-depleted NiAl(100) surface as displayed in figure 1. In the concentration regime between these two phases, a (1×1) structure occurred with, however, substantial surface disorder even after a careful annealing procedure as revealed by scanning tunnelling microscopy. A LEED intensity analysis performed for the latter structure [7] unambiguously identified the surface to be principally Al-terminated. Additionally, an admixture of 10% Ni atoms to the first layer was found as well as a 10% concentration of vacancies within the second layer, which is otherwise made up of Ni. Even though it has to be conceded that the overall sensitivity of LEED to the chemical constitution of the first two layers is roughly of the same order as the measured deviations from the ideal B2 stoichiometry, this result is quite remarkable. Instead of both defect types (Ni antisites *and* Ni vacancies) to be observed simultaneously, so far only the presence of a single constitutional defect type within the NiAl(100) surface has been taken into account.

In order to shed light upon the defect energetics within the NiAl(100) surface, we have performed first-principles calculations, in order to determine the relative stability of vacancies and antisites within the Ni and Al layers. As the most surprising result we will show in the following that a defect-free NiAl(100) surface is not a ground state at all. Instead, so-called Ni double-defects will be present at the surface even in the case of ideal stoichiometry.

2. Methodology

Density functional theory calculations were performed using the Vienna *ab initio* simulation package (VASP) [8–11] and ultrasoft pseudopotentials [12]. The exchange–correlation was treated within the generalized gradient approximation (GGA) according to Perdew *et al* (PW91) [13]. Application of this functional on bulk B2-NiAl results in a lattice parameter $a_0 = 2.898$ Å and a bulk modulus $B_0 = 1.54$ Mbar which are close to the experimental values ($a_0^{\mathrm{exp}} = 2.887$ Å [14], $B_0^{\mathrm{exp}} = 1.89$ Mbar [15]).

The NiAl(100) surface was modelled by repeated surface slabs of 5 NiAl bilayers and an additional layer (Ni or Al depending on slab termination) to symmetrize the slabs. They were separated by a vacuum equivalent to 4.5 NiAl bilayers, resulting in a total size of the supercell of 28.98 Å. The outermost four layers on each side of the symmetric slabs were relaxed, while the central three layers were kept at a bulk-like separation. Laterally, the surface slabs had dimensions of either (1×1) (ideal surface termination only), (2×2) or (3×3) atoms. For the determination of ground state energies, Brillouin zone sampling used a ($24 \times 24 \times 2$) Monkhorst–Pack mesh [16] for structures with a lateral (1×1) surface unit cell, and reciprocally less for structures with larger periodicities. In the bulk calculations, which are necessary to determine the segregation energy in equation (2), cubic bulk slabs made up of ($3 \times 3 \times 3$) B2 unit cells have been used.

To evaluate both the relative stability of defect configurations as well as the segregation behaviour of the different defect types, we focus on the calculation of two values, the surface formation energy and the defect segregation energy: The energy of surface formation ΔE_{surf} [17] can be defined as

$$\Delta E_{\mathrm{surf}} = \frac{1}{2A_{\mathrm{surf}}}\left(E_{\mathrm{tot}}(N^{\mathrm{Ni}}_{\mathrm{slab}}, N^{\mathrm{Al}}_{\mathrm{slab}}) - N^{\mathrm{Ni}}_{\mathrm{slab}} E_{\mathrm{tot}}(N^{\mathrm{Ni}}_{\mathrm{bulk}}) - N^{\mathrm{Al}}_{\mathrm{slab}} E_{\mathrm{tot}}(N^{\mathrm{Al}}_{\mathrm{bulk}}) - \Delta H_{\mathrm{f}}^{\mathrm{B2}}(N^{\mathrm{Ni}}_{\mathrm{slab}}, N^{\mathrm{Al}}_{\mathrm{slab}})\right). \quad (1)$$

It represents the difference of the total energy of the surface slab $E_{\mathrm{tot}}(N^{\mathrm{Ni}}_{\mathrm{slab}}, N^{\mathrm{Al}}_{\mathrm{slab}})$ (made up of $N^{\mathrm{Ni}}_{\mathrm{slab}}$ Ni and $N^{\mathrm{Al}}_{\mathrm{slab}}$ Al atoms) and the bulk energies $E_{\mathrm{tot}}(N_{\mathrm{bulk}})$ of the respective constituents as well as the enthalpy of formation of NiAl $\Delta H_{\mathrm{f}}^{\mathrm{B2}}(N^{\mathrm{Ni}}_{\mathrm{slab}}, N^{\mathrm{Al}}_{\mathrm{slab}})$. ΔE_{surf} is normalized to the surface area of the slab A_{surf}, which is given in units of the area of the (1×1) surface unit cell. When ΔE_{surf} is calculated for a set of arbitrary surface configurations $\sigma(x)$, a stability diagram can be constructed by plotting $\Delta E_{\mathrm{surf}}(x)$ for all evaluated configurations. The stable configurations are those which form the convex hull over all $\Delta E_{\mathrm{surf}}(x)$.

To determine whether defects are preferably located in the bulk or within the surface, we evaluate the segregation energy

$$\Delta E_{\mathrm{seg}} = \tfrac{1}{2}E_{\mathrm{tot}}(N^{\mathrm{Ni}}_{\mathrm{surf,def}}, N^{\mathrm{Al}}_{\mathrm{surf,def}}) - \tfrac{1}{2}E_{\mathrm{tot}}(N^{\mathrm{Ni}}_{\mathrm{surf,ideal}}, N^{\mathrm{Al}}_{\mathrm{surf,ideal}}) - \left(E^{\mathrm{bulk}}_{\mathrm{tot}}(N^{\mathrm{Ni}}_{\mathrm{surf,def}}, N^{\mathrm{Al}}_{\mathrm{surf,def}}) - E^{\mathrm{bulk}}_{\mathrm{tot}}(N^{\mathrm{Ni}}_{\mathrm{surf,ideal}}, N^{\mathrm{Al}}_{\mathrm{surf,ideal}})\right). \quad (2)$$

Here, $E_{\mathrm{tot}}(N^{\mathrm{Ni}}_{\mathrm{surf,def}}, N^{\mathrm{Al}}_{\mathrm{surf,def}})$ denotes the total energy of a surface slab, including a defect on either side of the symmetric slab, which is why the prefactor $\frac{1}{2}$ is required. $E_{\mathrm{tot}}(N^{\mathrm{Al}}_{\mathrm{surf,ideal}}, N^{\mathrm{Al}}_{\mathrm{surf,ideal}})$ is the energy of the ideal slab. From their energy difference, the difference between the energy of a single defect in a bulk slab $E^{\mathrm{bulk}}_{\mathrm{tot}}(N^{\mathrm{Al}}_{\mathrm{surf,def}}, N^{\mathrm{Al}}_{\mathrm{surf,def}})$ and the respective energy of an ideal bulk slab $E^{\mathrm{bulk}}_{\mathrm{tot}}(N^{\mathrm{Al}}_{\mathrm{surf,ideal}}, N^{\mathrm{Al}}_{\mathrm{surf,ideal}})$ is subtracted.

The values given for the segregation energies in section 3 have been computed for surface slabs with a lateral dimension of (3×3) atoms per layer and bulk slabs with a dimension of $(3 \times 3 \times 3)$ B2 unit cells.

3. Results

It has been shown in the past that for NiAl(100) the Al-termination is energetically favourable with respect to the Ni termination [17]. The same result has been obtained here, with a difference in the energy of surface formation of $\Delta E_{\mathrm{surf}}(x) = 0.34$ eV. Therefore, in this paper we will limit our investigations to point defects within an *Al-terminated* NiAl(100) surface.

The different defect types, which will be discussed, can be categorized into three groups.

(i) Ni defects, i.e. vacancies within an Ni layer and Ni atoms within an Al layer (Ni antisites); these two defects are the constitutional defect type for bulk NiAl.
(ii) Al defects, i.e. vacancies within an Al layer and Al atoms within an Ni layer (Al antisites).
(iii) Multi-defects, i.e. combinations of two point defects.

Concerning multi-defects, we want to limit this study to the evaluation of combinations of Ni antisites with Ni vacancies in order to find reasons for their suggested experimental observation [7].

3.1. Nickel defects

Among the different point defects, the study of Ni vacancies within Ni layers as well as Ni antisites within Al layers is particularly interesting, not only because these two defects have been observed in the above mentioned LEED structure analysis [7], but also because those two defects are the constitutional defect types in off-stoichiometric NiAl crystals. Due to imperfections occurring during crystal growth and surface preparation, such off-stoichiometries cannot be avoided. Thus any experimental observation is based on samples which exhibit deviations from the ideal Ni concentration of $x = 0.5$, and thereby contain either a certain quantity of vacancies on the Ni sublattice or Ni antisites on the Al sublattice of the B2 structure. The bulk, and especially the near-surface part of the bulk, which lies close enough to the surface for defects to migrate into the surface, do thus represent a reservoir of defects, which is coupled to the surface [18].

In table 1 we present the results obtained for all inequivalent configurations of up to two Ni antisites with a lateral periodicity of (2×2) and (3×3), within the first or the third layer. For configurations, which include a higher number of defects per supercell $n_{\mathrm{def}} > 1$, their relative distance d is given as a function of the lattice constant a_0 of NiAl, which corresponds to the in-plane nearest-neighbour distance.

Table 1. Energetics of Ni antisites within Al layers as determined by density functional theory. Calculations were performed for defect configurations located within the first or third layer and lateral periodicities of (2×2) or (3×3) surface slabs. $x_{4\mathrm{L}}$ corresponds to the Ni concentration within the first four layers. The configuration, which is referred to as $d =$ 'diag.', is a diagonal order of Ni antisites in the first layer, which results in a c($\sqrt{2} \times 3\sqrt{2}$)R45° order, also observed in experiment. Energies are given in eV.

Periodicity	n_{def}	Location	d	$x_{4\mathrm{L}}$	ΔE_{surf}
Ideal B2	0	—	—	0.500	1.019
(2×2)	1	1st layer	—	0.563	1.158
(2×2)	1	3rd layer	—	0.563	1.240
(2×2)	2	1st layer	$\sqrt{2}a_0$	0.625	1.362
(2×2)	2	1st layer	a_0	0.625	1.483
(2×2)	2	3rd layer	$\sqrt{2}a_0$	0.625	1.481
(2×2)	2	3rd layer	a_0	0.625	1.528
(3×3)	1	1st layer	—	0.528	1.029
(3×3)	1	3rd layer	—	0.528	1.092
(3×3)	2	1st layer	$\sqrt{2}a_0$	0.556	1.081
(3×3)	2	1st layer	a_0	0.556	1.126
(3×3)	2	3rd layer	$\sqrt{2}a_0$	0.556	1.189
(3×3)	2	3rd layer	a_0	0.556	1.206
(3×3)	3	1st layer	diag.	0.583	1.151

These results show a few interesting features: first of all, the incorporation of a defect within the first layer results in a lower surface energy ΔE_{surf} than if the defect is introduced into the third layer—independent of the actual configuration of the defect. Furthermore, when comparing different configurations of defects, which have the same Ni concentration $x_{4\mathrm{L}}$ within the first four layers, a relative distance of $d = \sqrt{2}a_0$ between the defect proves to be more stable than $d = a_0$. Thus an alignment along either one of the surface's unit-cell vectors is energetically less favourable than a diagonal arrangement of Ni antisites. This is in line with the experimental observation of a c($\sqrt{2} \times 3\sqrt{2}$)R45° phase on the NiAl(100) surface, which also consists of a diagonal arrangement of defects, as can be seen in figure 1(left). Such a c($\sqrt{2} \times 3\sqrt{2}$)R45° order of Ni antisites, equivalent to the configuration 'diag' in the last row of table 1, does even lead to a lower energy of surface formation than a single antisite in a (2×2) order, although the latter's defect density is lower. While the energy difference between the two configurations is rather small (7 meV), this finding is in line with experiment, where no signs of a (2×2)-like order are found.

The embedding of Ni vacancies within the second or fourth layer exhibits almost the same features as for Ni antisites. Table 2 shows that the presence of these defects within the second layer (which is the outermost Ni layer) is preferential to the defects located within the fourth layer. We also find the same preference for a diagonal ordering of the vacancies within a layer. This preference is so strong that a c($\sqrt{2} \times 3\sqrt{2}$)R45° order of three Ni vacancies within the second layer leads to an energy of surface formation, which is practically the same than for the ideal B2 surface.

Table 2. The same as table 1, but for Ni vacancies within Ni layers (second and fourth layer). All energies are given in eV.

Periodicity	n_{def}	Location	d	$x_{4\mathrm{L}}$	ΔE_{surf}
Ideal B2	0	—	—	0.500	1.019
(2×2)	1	2nd layer	—	0.467	1.050
(2×2)	1	4th layer	—	0.467	1.152
(2×2)	2	2nd layer	$\sqrt{2}a_0$	0.429	1.170
(2×2)	2	2nd layer	a_0	0.429	1.236
(2×2)	2	4th layer	$\sqrt{2}a_0$	0.429	1.251
(2×2)	2	4th layer	a_0	0.429	1.362
(3×3)	1	2nd layer	—	0.486	1.021
(3×3)	1	4th layer	—	0.486	1.064
(3×3)	2	2nd layer	$\sqrt{2}a_0$	0.471	1.024
(3×3)	2	2nd layer	a_0	0.471	1.061
(3×3)	2	4th layer	$\sqrt{2}a_0$	0.471	1.101
(3×3)	2	4th layer	a_0	0.471	1.141
(3×3)	3	2nd layer	diag.	0.455	1.020

For the segregation of Ni antisites from the bulk, to the first layer, a segregation energy of $\Delta E_{\mathrm{seg}} = -1.034$ eV is obtained. This means that every excess Ni atom located near the surface within a relatively dilute concentration of one antisite atom within 27 B2 unit cells can gain as much as 1 eV, if it segregates to the surface. Thus, as soon as sufficient activation energy is provided for migration, e.g. during the preparation of the surface, a large quantity of defects from the bulk will be driven into the first layer.

The evaluation of the segregation energy for Ni vacancies leads to a value of $\Delta E_{\mathrm{seg}} = -0.290$ eV. Even though this is only about a third of the value obtained for Ni antisites, it is certainly sufficient to strongly attract vacancies into the second layer. It can be concluded that both constitutional defects show a pronounced (though not equally strong) preference for segregation to the surface from the bulk and will thus be found in much higher concentrations within the outermost layers. The same behaviour has already been observed for CoAl(100) and referred to as the 'magnifying glass effect' of the surface on off-stoichiometries in the bulk [18].

3.2. Aluminium defects

Neither Al antisites on the Ni sublattice nor Al vacancies on the Al lattice are found to be constitutional defects in the bulk, and thus they only occur in concentrations about two orders of magnitude below the concentrations of Ni defects [19]. Also in the recent LEED analysis [7], no signs of Al defects are found. Nevertheless, there has been disagreement in the past, whether the $\mathrm{c}(\sqrt{2}\times3\sqrt{2})\mathrm{R45}^\circ$ superstructure consists of diagonal arrangements of Ni antisites or Al vacancies, as pointed out in the introduction. For these reasons, a small set of configurations of Al defects have also been calculated, in order to show general trends of their stability with respect to other defect types.

Table 3 displays the energetic properties of Al antisites and Al vacancies within the first four layers. As expected, the values obtained for Al antisites show that this is clearly not the stable defect type for Ni-deficient surfaces ($x < 0.5$).

Table 3. The same as tables 1 and 2 but for Al antisites and Al vacancies within the first four layers. Energies are given in eV.

Periodicity	n_{def}	Location	d	$x_{4\mathrm{L}}$	ΔE_{surf}
Al antisites					
(2×2)	1	2nd layer	—	0.438	1.417
(2×2)	1	4th layer	—	0.438	1.447
(3×3)	1	2nd layer	—	0.472	1.182
(3×3)	1	4th layer	—	0.472	1.203
Al vacancies					
(2×2)	1	1st layer	—	0.533	1.063
(2×2)	1	3rd layer	—	0.533	1.408
(3×3)	1	1st layer	—	0.514	1.022
(3×3)	3	1st layer	diag.	0.545	1.110

The energy of surface formation, resulting from the embedding of this defect in the surface, is roughly 0.1 eV higher than for a surface of the same Ni concentration $x_{4\mathrm{L}}$, which instead includes Ni vacancies. Therefore, it is only of minor interest to note that there is just a slight preference for the Al antisites to be located in the second rather than the fourth layer.

In contrast to this, Al vacancies are surprisingly found to exhibit almost the same energy of surface formation when occurring in a low concentration of $x_{4\mathrm{L}} = 0.514$ within the surface. Nevertheless this changes for higher defect concentrations, where Al vacancies are less stable than the formation of Ni antisites within the first layer. Therefore, the *ab initio* results do not corroborate the existence of a long-range-ordered $\mathrm{c}(\sqrt{2}\times3\sqrt{2})\mathrm{R45}^\circ$ phase of Al vacancies (figure 1 (right)) as proposed in [6].

Concerning the segregation energy, values of $\Delta E_{\mathrm{seg}}^{\mathrm{Alanti}} = -0.093$ eV and $\Delta E_{\mathrm{seg}}^{\mathrm{Alvac}} = -1.727$ eV are obtained for Al antisites and vacancies, respectively. While the segregation energy shows only a weak preference for the location of an antisite in the surface, this is very pronounced for the Al vacancy. Nevertheless, the impact of this result on Al vacancies in the bulk should not be overestimated. As mentioned above, there are only a very few Al vacancies found in bulk NiAl [19]. Furthermore, every Al vacancy, which is created in the bulk is more likely to break up into an Ni vacancy and an Ni antisite—a process which is energetically favourable by 0.5 eV— than to migrate to the surface. Thus, if any Al vacancies would be found in the surface, they are more likely to have been created in the surface than segregated to the surface from the bulk.

3.3. Double defects

Motivated by the results of the recent LEED structural analysis [7] mentioned in the introduction, we have also investigated the energetic properties of the coexistence of the two Ni defect types. They are presented in table 4.

The astonishing result is that there are two configurations of Ni double-defects, which result in a lower energy of surface formation than the ideal B2 surface: a single double-defect within a (3×3) periodicity, as well as a $\mathrm{c}(\sqrt{2}\times3\sqrt{2})\mathrm{R45}^\circ$ order of three double-defects. Furthermore the results show that the double defects are energetically most stable within

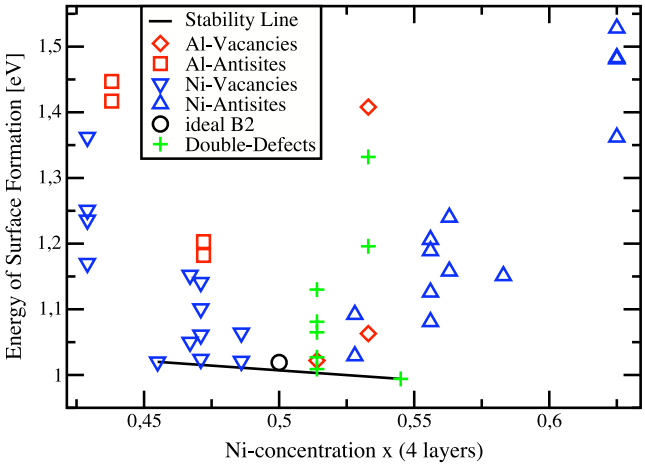

Figure 2. Stability diagram $\Delta E_{\mathrm{surf}}(x)$, including all defect concentrations, presented in tables 1–4. It can be seen that the ideal B2-(1 × 1) phase is unstable and energy can be gained by breaking it up into two domains with a c($\sqrt{2} \times 3\sqrt{2}$)R45° order of Ni vacancies and Ni double-defects, respectively.

(This figure is in colour only in the electronic version)

Table 4. The same as table 1, but for Ni double-defects, i.e. Ni antisites within the first or third layer and Ni vacancies within the second or fourth layer. Energies are given in eV.

Periodicity	n_{def}	Location	d	$x_{4\mathrm{L}}$	ΔE_{surf}
Ideal B2	0	—	—	0.500	1.019
(2 × 2)	1	1st/2nd layer	$\sqrt{3}/2a_0$	0.533	1.196
(2 × 2)	1	3rd/4th layer	$\sqrt{3}/2a_0$	0.533	1.332
(3 × 3)	1	1st/2nd layer	$\sqrt{3}/2a_0$	0.514	1.009
(3 × 3)	1	1st/2nd layer	$\sqrt{19}/2a_0$	0.514	1.027
(3 × 3)	1	1st/2nd layer	$\sqrt{11}/2a_0$	0.514	1.065
(3 × 3)	1	1st/2nd layer	$\sqrt{3}/2a_0$	0.514	1.081
(3 × 3)	1	3rd/4th layer	$\sqrt{3}/2a_0$	0.514	1.130
(3 × 3)	3	1st/2nd layer	diag.	0.545	0.994

the first two layers and that the nearest-neighbour distance of $\sqrt{3}/2a_0$ results in a lower energy than if the two point defects are separated further from each other.

4. Discussion and conclusion

The results that have been obtained for the various defect types have been mapped in a stability diagram, displayed in figure 2. As the evaluation of possible defect configurations is far from being exhaustive, the actual stability line has only been drawn in between the two defect configurations which have been found to be stable. This stability diagram exhibits two rather unexpected features:

The first surprising result is that, for Ni-rich NiAl(100) surfaces, we do not find a single defect type to be dominant at the surface. Instead, the existence of a so-called Ni double-defect consisting of an Ni vacancy in the second layer and an Ni antisite in the first layer turns out to be more stable than either a solitary Ni antisite or Al vacancy. This finding contrasts with the behaviour of the CoAl(100) surface, where only Co antisites are present at the surface [1, 18]. As surprising as this may seem, it is in line with the experimental findings [7], where simultaneously 10% Ni vacancies within the second layer and 10% Ni antisites within the first layer are found by LEED analysis.

The second surprise is that the surface formation energy of the ideal B2 structure lies above the stability line drawn between the two stable c($\sqrt{2} \times 3\sqrt{2}$)R45° structures displayed in figure 3. This means that the ideal Al-terminated NiAl(100)-(1 × 1) surface is *not* the stable configuration, even for an ideal stoichiometric crystal. Instead, the stable configuration is a 50:50 mixture of the two c($\sqrt{2} \times 3\sqrt{2}$)R45° structures. The same holds for the whole concentration range $0.455 \leqslant x_{4\mathrm{L}} \leqslant 0.545$. In the thermodynamic ground state, every NiAl(100) surface, whose first four layers have a concentration within this range, decomposes into two domains with the same c($\sqrt{2} \times 3\sqrt{2}$)R45° order, but different defects—Ni vacancies in one domain and Ni double-defects in the other. The relative weight of each domain is determined by the actual Ni concentration of the surface. Any other surface configuration can only be metastable.

This explains why the only consistent feature of all experimental studies is a c($\sqrt{2} \times 3\sqrt{2}$)R45° ordering of

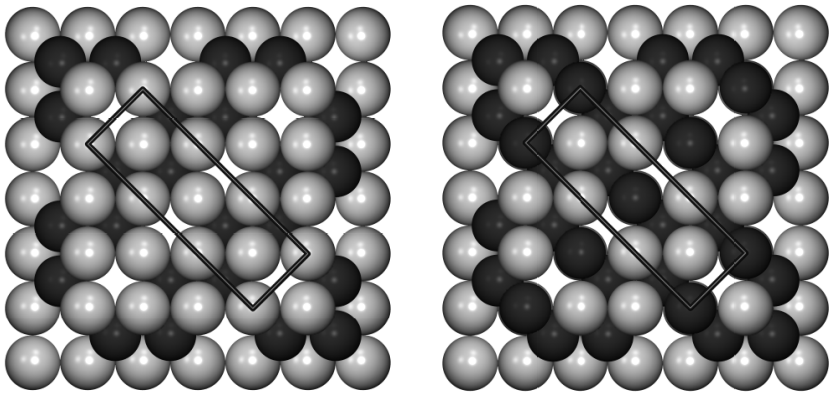

Figure 3. Illustration of the c($\sqrt{2} \times 3\sqrt{2}$)R45° order of vacancies within the second layer (left) and Ni double-defects within the first two layers (right), which are found to be the two stable defect configurations of NiAl(100).

defects, as this order is stable for a comparably wide range of surface compositions. Concerning the actual defect type found in the surface, none of the experimental results can be fully corroborated by this *ab initio* study. The formation of this surface structure through Ni antisites arranged diagonally within the first layer, as reported by Mullins and Overbury [5], is only stable when, in addition, Ni vacancies are present in the second layer, being ordered in the same way. The resulting diagonal arrangement of Ni double-defects within the first two layers is illustrated in figure 3 (right). On the other hand, the formation of a diagonal arrangement of Al vacancies as reported by Blum *et al* [6] is found to be unstable with respect to such a c($\sqrt{2} \times 3\sqrt{2}$)R45° order of double defects.

According to these results, every observation of a (1×1) surface must be due to an insufficient annealing process, which prohibits the complex formation of a long-range-ordered c($\sqrt{2} \times 3\sqrt{2}$)R45° structure. This is in line with the observations of Blum *et al* [6], where the Al-terminated (1×1) structure does only appear for annealing temperatures below 500 K. More heat of activation leads to the formation of a c($\sqrt{2} \times 3\sqrt{2}$)R45° order of the defects, which have to be present within the (1×1) surface. The appearance of an Ni-terminated (1×1) phase can be attributed to the fact that Al sublimates the surface at lower temperatures than Ni.

In general, this work demonstrates how theoretical studies based on electronic structure theory can be very helpful in understanding the stability of compound surfaces and in solving apparent disagreements between experimental results. Here, the (100) surface of B2-NiAl is another example for our statement that surface segregation in intermetallic compounds is more the rule than the exception.

Acknowledgment

The first author thanks the Studienstiftung des deutschen Volkes for financial support.

References

[1] Blum V, Hammer L, Schmidt Ch, Meier W, Wieckhorst O, Müller S and Heinz K 2002 *Phys. Rev. Lett.* **89** 266102
[2] Müller S, Stöhr M and Wieckhorst O 2005 *Appl. Phys.* A **82** 415
[3] Davis H and Noonan J 1987 *Mater. Res. Soc. Symp.* **83** 3
[4] Davis H and Noonan J 1988 *Springer Series in Surface Sciences* vol 1 (Berlin: Springer) p 152
[5] Mullins D R and Overbury S H 1988 *Surf. Sci.* **199** 141
[6] Blum R-P, Ahlberendt D and Niehus H 1996 *Surf. Sci.* **366** 107–20
[7] Lerch D, Schurr R, Hammer L, Müller S and Heinz K 2009 unpublished
[8] Kresse G and Hafner J 1993 *Phys. Rev.* B **47** 558
[9] Kresse G and Hafner J 1994 *J. Phys.: Condens. Matter* **6** 8245
[10] Kresse G and Furthmüller J 1996 *Phys. Rev.* B **54** 11169
[11] Kresse G and Furthmüller J 1996 *Comput. Mater. Sci.* **6** 15
[12] Vanderbilt D 1990 *Phys. Rev.* B **41** 7892–5
[13] Perdew J P and Wang Y 1992 *Phys. Rev.* B **45** 13244
[14] Freeman A J, Hong T, Lin W and Xu J H 1991 *High Temperature Intermetallics* vol IV (Pittsburgh, PA: Materials Research Society)
[15] Villars P and Calvert L D 1985 *Pearson's Handbook of Crystallographic Data for Intermetallic Phases* vol 1–3 (Metals Park, OH: American Society of Metals)
[16] Monkhorst H J and Pack J D 1976 *Phys. Rev.* B **13** 5188
[17] Müller S 2003 *J. Phys.: Condens. Matter* **15** 1429
[18] Wieckhorst O, Müller S, Hammer L and Heinz K 2004 *Phys. Rev. Lett.* **92** 195503
[19] Fu C L, Ye Y-Y, Yoo M H and Ho K M 1993 *Phys. Rev.* B **48** 6712–5